Estimation of Longitudinal Wakefield Effects in the TESLA-TTF FEL undulator beam pipe and diagnostic section

Martin Dohlus[1]), Ronald Lorenz[2]), Thorsten Kamps[2]),
Holger Schlarb[1]), Rainer Wanzenberg[1])

[1]) DESY, Notkestr. 85, 22603 Hamburg,
[2]) DESY, Platanenallee 6, 15738 Zeuthen

March 17, 1998

Abstract

An Electron beam with a small energy spread (0.1 %) is required to drive a Free Electron Laser at the TTF at DESY. During the FEL-process wakefields are generated by several components, which will induce an additional energy spread in the beam. The longitudinal wakefields due to the resistivity and surface roughness of the undulator pipe, the beam positions monitors, and the diagnostic station are estimated. A list of all contributions is presented for an rms bunch length of 50 μm and 250 μm and two phases of the project. The contribution due to the surface roughness can be large for the Phase II (50 μm bunch length). It is expected that the correlated energy spread (peak value) will exceed 0.1 % for that case.

1 Introduction

The construction of a free-electron laser (FEL) based on the self-amplified spontaneous emission mechanism (SASE) is under way at DESY [1]. The goal is to obtain a coherent, very bright beam of photons with wavelengths tunable between 6 and 20 nm. The high intensity electron beam needed to drive the undulator will be delivered by the TESLA Test Facility Linac (TTFL). Some parameters for the FEL-operation of the TTFL are listed in Table 1. In Phase I the undulator consists of three identical modules, each containing a 4.5 m long vacuum chamber

made of aluminum. The energy of the electron beam delivered by the TTFL will be 380 MeV. For Phase II three additional modules will be installed, the bunch length will be compressed down to about 50 μm and the energy will be 1 GeV. The three undulator modules of Phase I are shown in Fig. 1, together with their

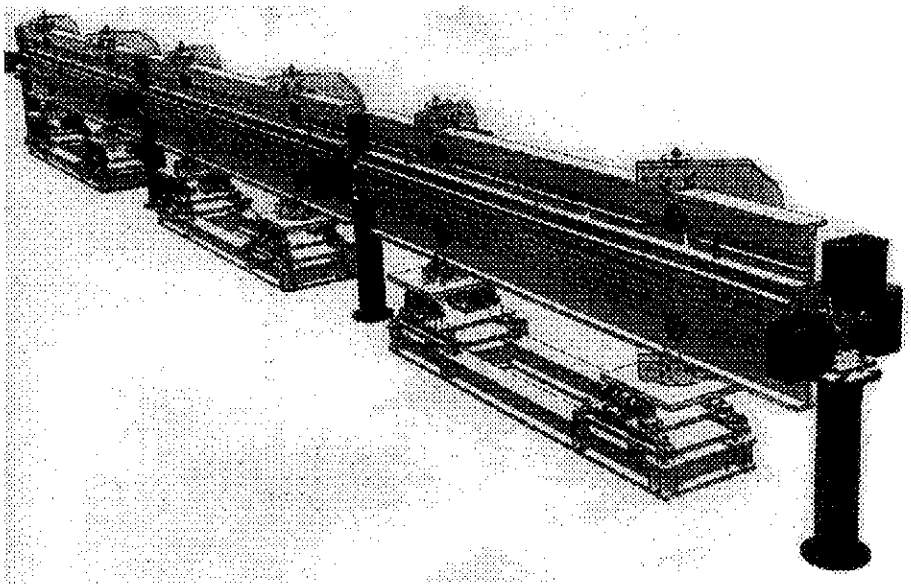

Figure 1: TESLA-TF FEL undulator, Phase I

girders and four diagnostic stations. Each diagnostic station contains two cavity beam position monitors, two wire scanners and pumping slots.

Beam energy, Phase I / II	380 MeV / 1000 MeV
Bunch length (σ_z), Phase I / II	250 μm / 50 μm
Bunch charge	1 nC
Spacing of the 7200 bunches	111 ns
Repetition rate	10 Hz

Table 1: Parameters for the TTFL-FEL.

This paper will look at the wakefield effects in the undulator sections. These wakefields will generate a *changing* correlated energy spread. Initially the bunch will have an uncorrelated energy spread, for example due to the effects in the bunch compressors, and a correlated energy spread due to the wakefields in the linac of the TTF. A small uncorrelated energy spread of 0.1 % is required for the chosen FEL parameters [1, Sect. 1.4.2]. During the SASE-FEL process wakefields in the undulator pipe and diagnostic section will change the correlated energy

spread in the bunch. The peak value of that change at the end of the last undulator section is given in table 12, which summarizes all the following results. It is expected that a correlated, or even an adiabatically changing correlated, energy spread will have a less important impact on the FEL gain than an uncorrelated one. Nevertheless we will take the value of 0.1 % as a reference for the correlated energy spread, too.

2 Undulator pipe

2.1 Resistive wall wake

The wakefields due to the finite resistivity of a beam pipe are very important for small bunches. Here we use the results obtained by K. Bane, [2]. The resistive wall wake of a round pipe of length l is given by an analytical expression:

$$W_{rwall}(s) = \frac{4}{\pi}\frac{Z_0\, c}{b^2}\; F_{rwall}(s/\sigma_z, \sigma_z/s_0)\; l \qquad (1)$$

s_0 is a material dependent characteristic length, b is the beam pipe radius, $Z_0 = 377\ \Omega$, and c the velocity of light.

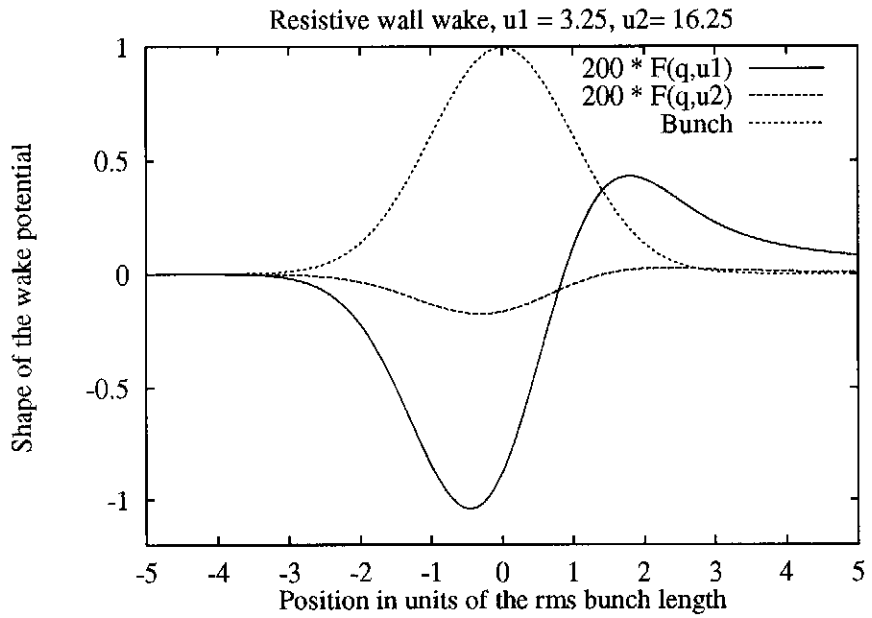

Figure 2: Resistive wall wake. The function $200 \cdot F(q = s/\sigma_z, u)$ is show for two values of u: $u_1 = 50\ \mu\mathrm{m}/s_0$ and $u_1 = 250\ \mu\mathrm{m}/s_0$.

The undulator beam pipe will be manufactured from aluminum. Using the conductivity of $\sigma_{Al} = 36.59 \cdot 10^6\ (\Omega\,\mathrm{m})^{-1}$ for aluminum at room temperature and

a pipe radius of $b = 5$ mm one finds:

$$s_0 = \left(\frac{2\,b^2}{\sigma_{Al}\,Z_0}\right)^{1/3} = 15.4\,\mu\text{m}, \tag{2}$$

and for the factor in front of the function F_{rwall}:

$$\hat{W}'_{rwall} = \frac{4\;Z_0\,c}{\pi\;b^2} = 200\;\cdot\;28.76\frac{\text{kV}}{\text{nC}\;\cdot\;\text{m}}$$

The function $F_{rwall}(q, u_0)$ depends on the ratios $q = s/\sigma_z$ and $u_0 = \sigma_z/s_0$, and can be written as a convolution integral of a Gaussian bunch (σ_z is the rms length) and a point charge Greens function $f(v)$.

$$F_{rwall}(q, u_0) = -\int_0^\infty dq'\;\frac{1}{\sqrt{2\,\pi}}\;\exp(-\frac{1}{2}\,(q-q')^2)\;\;f(u_0\,q). \tag{3}$$

The point charge Greens function $f(v)$ has been calculated in [2]:
$f(v) = 1/3\;\exp(-v)\;\cos(\sqrt{3}\,v)\;-\sqrt{2}/\pi\;\int_0^\infty dv'\,v'^2\exp(-v\,v'^2)/(8+v'^8)$.

The shape and the amplitude of the wake field depends on the ratio σ_z/s_0. Fig. 2 shows the function $200\;\times\;F_{rwall}(q, u_0)$ for $u_0 = 50\;\mu\text{m}/s_0 = 3.24$ and $u_0 = 250\;\mu\text{m}/s_0 = 16.25$. The peak wake of the 250 μm bunch is by a factor of 6 smaller than the wake of the 50 μm long bunch. A detailed discussion of resistive wall wakefields for an extensive range of parameters can be found in [3].

The length of the beam pipe in one undulator section is about 4.5 m. The contribution due to the resistivity of the aluminum beam pipe for **one** undulator section is summarized in the following table 2:

length	bunch length	
	50 μm	250 μm
per unit length	28.8 kV/(nC m)	4.8 kV/(nC m)
one module (4.5 m)	129.6 kV/nC	21.6 kV/nC

Table 2: Peak wake potential of the contribution from the resistive wall of one undulator module.

2.2 Surface Roughness and Oxide Layers

The impedance of a perfectly conducting beam-pipe covered with a longitudinally uniform thin dielectric layer can be calculated analytically [5]. For the surface roughness different models exist. One is based on the impedance of a dielectric layer with an effective thickness. The oxide layers of the aluminum undulator pipe are 1.5 to 2 nm thick, while the rms surface roughness is 350 nm [6].

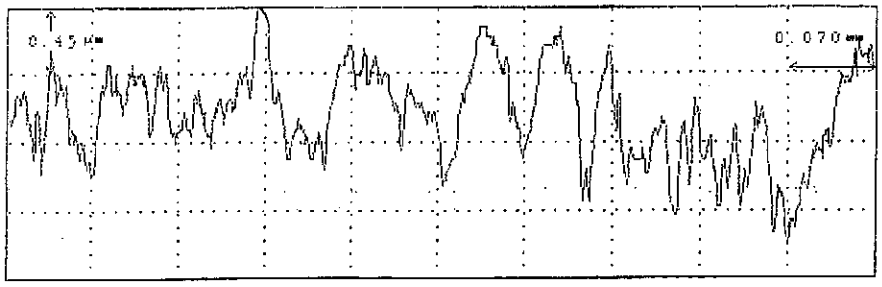

Figure 3: Measured surface roughness of a piece of the undulator pipe. The abscissa is the longitudinal position along the pipe (0.07 mm per division), while the ordinate represents the radius of the pipe (0.45 μm per division). The rms surface roughness is $\sigma_{RA} = 350$ nm [6].

2.3 Oxide Layers

The analytic expression for the impedance per unit length of a perfectly conducting beam-pipe covered with a longitudinally uniform thin dielectric layer of thickness δ and permittivity ϵ_r is given by

$$Z_{\parallel}(\omega) = \frac{Z_0\, c}{\pi b^2} \frac{1}{i\omega_r \left(\frac{\omega_r}{\omega} - \frac{\omega}{\omega_r}\right)} = -i\,\omega \frac{Z_0\, c}{\pi\, b^2\, {\omega_r}^2} \frac{1}{1 - \left(\frac{\omega}{\omega_r}\right)^2} \tag{4}$$

with a resonance frequency of

$$\omega_r \approx c\sqrt{\frac{2\epsilon_r}{(\epsilon_r - 1)\delta b}} \tag{5}$$

The wake potential of a Gaussian bunch obtained from the above impedance is ($k_r = \omega_r/c$)

$$W_{diele}(s) = \frac{Z_0 c}{\pi b^2}\, F_{diele}(s/\sigma_z, k_r\,\sigma_z)\; l, \tag{6}$$

for a pipe of length l and radius b. The function $F_{diele}(q,u)$ is defined as the convolution integral of the Gaussian bunch with the cosine wake potential of the excited mode:

$$F_{diele}(q,u) = -\int_0^\infty dq'\, \frac{1}{\sqrt{2\,\pi}} \exp(-\frac{1}{2}\,(q-q')^2)\;\; \cos(u\,q'). \tag{7}$$

Fig. 6 shows the function $u^2 \cdot F_{diele}(q,u)$ for different values of $u = \sigma_z\, k_r$.

In case of $k_r \gg 1/\sigma_z$ as expected for oxide layers at the vacuum chamber wall the wake potential turns out to be purely inductive and reduces to

$$W'_{diele}(s) = \frac{Z_0 c}{\pi b} \frac{(\epsilon_r - 1)\delta}{2\epsilon_r} \frac{s}{\sqrt{2\pi}\sigma_z^3} \exp\,(-\frac{s^2}{2\sigma_z^2}), \tag{8}$$

i.e. the function $F_{diele}(q,u)$ is approximated according to:

$$F_{diele}(q,u) \approx \frac{1}{u^2}\, q\, \frac{1}{\sqrt{2\,\pi}}\, \exp(-\frac{1}{2}\, q^2), \qquad u \gg 1. \tag{9}$$

Fig. 4 shows this approximation of the function $F_{diele}(q,u)$.

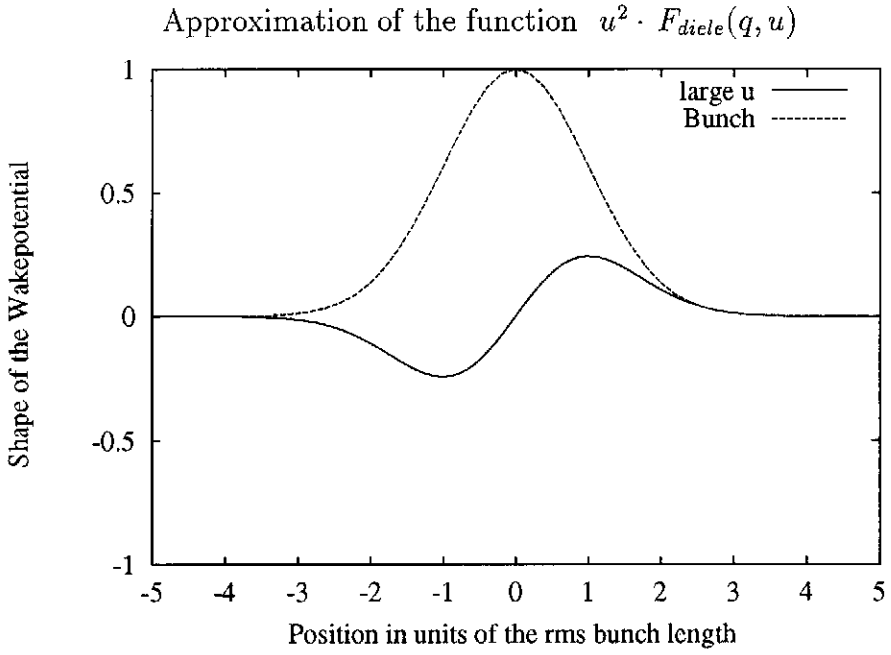

Figure 4: The approximation of the function $u^2 \cdot F_{diele}(q,u)$ is show for $u \gg 1$. This corresponds to a very thin oxide layer on the chamber wall.

The permittivity of Al_2O_3 is $\epsilon_r \approx 10$ [7]. The approximation for $F_{diele}(q,u)$, see Eqn.(9), can be used since, for a rms bunch length of 50 μm, a pipe radius of 5 mm and very thin layers (< 2 nm), the parameter u is much larger then unity ($u = k_r\,\sigma_z > 20$). The peak value of the wake potential can be found at the bunch position $s/\sigma_z = 1$:

$$\hat{W}_{diele} = \frac{Z_0\, c}{\pi}\, \frac{\exp(-0.5)}{\sqrt{2\,\pi}}\, \frac{(\epsilon_r - 1)}{2\epsilon_r}\, \frac{\delta\, l}{b\,\sigma_z^2} = 3.915 \frac{\mathrm{V\ m}}{\mathrm{nC}}\, \frac{\delta\, l}{b\,\sigma_z^2} \tag{10}$$

for $\epsilon_r = 10$.

The contribution due to an oxide layer is listed in table 3. The wakefields due to a very thin oxide layer are much smaller than the wakefields due to the resistivity of the material.

length	bunch length 50 μm	250 μm
per unit length	0.63 kV/(nC m)	0.025 kV/(nC m)
one module (4.5 m)	2.81 kV/nC	0.133 kV/nC

Table 3: Peak wake potential of the contribution from an oxide layer of the undulator pipe. The parameters $\epsilon_r = 10$ and $\delta = 2$ nm have been used.

2.4 Surface Roughness

2.4.1 2D Surface Roughness

A model for wakefields induced by small protrusions has been developed in [8]. According to this model the wakefields due to surface roughness in the steady state regime can be described by a thin dielectric layer. Numerical simulation of a large number of cylindrical symmetric protrusions show that, if δ is fixed by two times the RMS-value σ_{RA} of the surface roughness, ϵ_r will be given in the order of 2 but depends in principle on the shape of the protrusions. By using the code ABCI [9] the permittivities for two different shapes shown in Fig. 5 are given in table 4. A pipe radius of $b = 2$ mm has been used to keep the computing effort in reasonable limits.

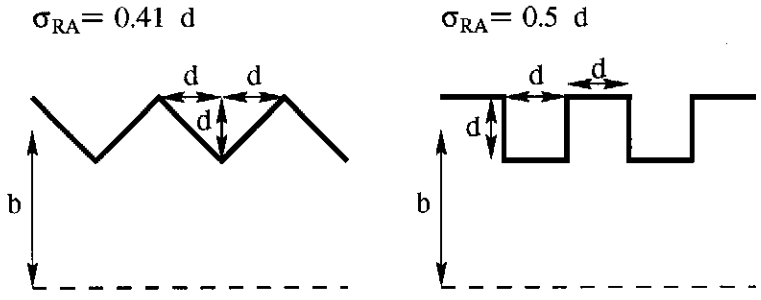

Figure 5: Shapes of protrusion used for numerical simulation

The surface roughness of the aluminum chamber has been measured to be $\sigma_{RA} = 350$ nm. The contribution of the wakefields due the surface roughness represented by a dielectric layer of permittivity $\epsilon_r = 1.5$ and a thickness $\delta = 2 \cdot \sigma_{RA}$ is listed in table 5.

	permittivity	
	triangular shape	rectangular shape
ϵ_r	1.465	1.830

Table 4: Permittivities ϵ_r calculated from numerical simulations ($\sigma_z = 250\,\mu$m, radius $b = 2\,$mm) for small rectangular and for small triangular (both $d = 50\,\mu$m) protrusions.

With an effective roughness, defined as

$$\delta_{eff} = \frac{(\epsilon_r - 1)}{2\,\epsilon_r}\,2\,\sigma_{RA}, \tag{11}$$

it is possible to write:

$$u = k_r\,\sigma_z = \frac{\sigma_z}{\sqrt{\delta_{eff}\,b}} \tag{12}$$

(where b is the radius of the pipe). According to the model used in table 5 one obtains: $\delta_{eff} = \sigma_{RA}/3$ and $u = 2.07$ (10.35) for a bunch length of $\sigma_z = 50\,\mu$m ($250\,\mu$m). Fig. 6 shows the shape of the wake potential for different values of $u = k_r\,\sigma_z$.

	bunch length	
	50 μm	250 μm
roughness $\epsilon_r = 1.5$, $\sigma_{RA} = 350\,$nm	120.7 kV/(nC m)	3.5 kV/(nC m)

Table 5: Peak wake potential of the contribution from the surface roughness of the undulator pipe for the 2D model of the surface roughness, using a dielectric layer. The peak values correspond to the minimum of the wake potential near the bunch center.

It should be mentioned that in both the numerical simulation and the analytical calculation a perfect conducting outer wall is assumed. However, for a bunch length of $250\,\mu$m the typical penetration depth of the electro-magnetic field into the wall is of the same order as the surface roughness. Then both effects cannot be calculated separately.
Secondly, the numerical simulations with the ABCI code [9] are limited to cylindrically symmetric beam pipes. The influence due to small protrusions of finite azimuthal angle cannot be computed with ABCI. These can only be calculated analytically in the non-steady-state regime by using a inductive wakefield model

[10]. For cylindrically symmetric structures and a small number of protrusions this model is in good agreement with numerical results.

The next section will study 3D periodic and 3D random models for the surface roughness.

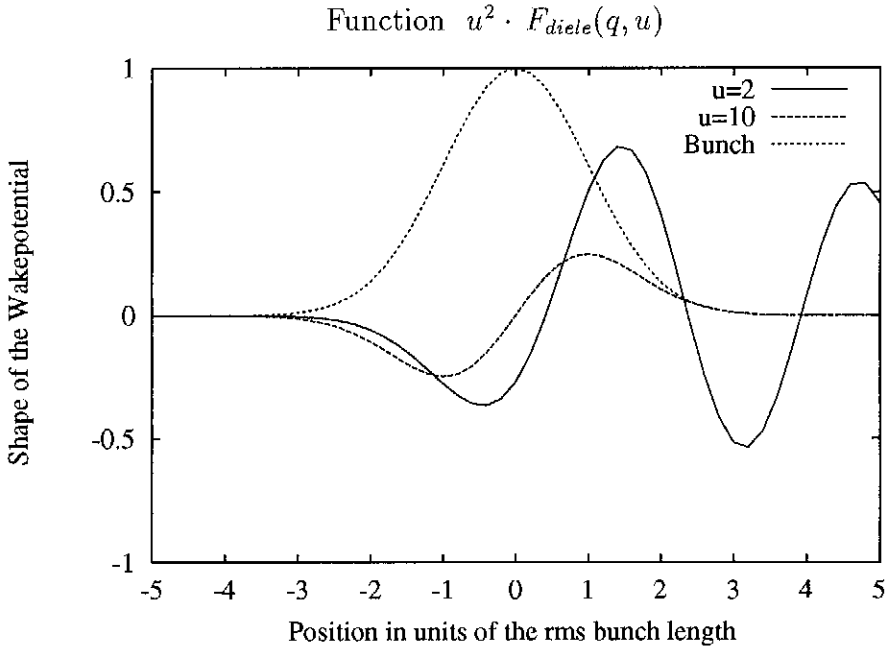

Figure 6: The function $u^2 \cdot F_{diele}(q,u)$ is show for different values of u.

2.4.2 3D Surface Roughness

To estimate the effects of real three dimensional surface roughness, the wakes of the surfaces shown in Fig. 7 have been calculated with the MAFIA T3 solver [4, 11]. For this purpose the inner surface of the pipe $(b+\delta r(\phi,z),\phi,z)$ has been transformed into a flat plane $(x=b+\delta r(y/b,z),y,z)$. The modified configuration is stimulated by a flat beam which causes the same surface fields (E_x, B_y) as would occur in the $r\phi z$ setup (E_r,B_ϕ).

Comparison of rz- and xz-model: The longitudinal impedance per unit length of beam pipe which is covered by one or more homogeneous layers can be written as

$$Z_{||}(\omega) = \frac{1}{2\pi b}\,\frac{-Z_s(\omega)}{1+\alpha b\frac{i\omega}{c}\frac{Z_s(\omega)}{Z_0}} \tag{13}$$

with $\alpha = 1/2$ for rz-geometry and $\alpha = 1$ for xz-geometry. $Z_s(\omega)$ is the surface impedance which relates perpendicular E- and H-field components:

$$Z_s(\omega) = \sqrt{\frac{\sigma}{i\omega\mu}\frac{\sigma - i\omega\varepsilon}{\sigma}} \tag{14}$$

for resistive beam pipes with $\delta_{\text{skin}} \ll b$ (σ is the conductivity of the pipe), and

$$Z_s(\omega) = i\omega L \quad \text{with} \quad L = \mu\delta\frac{\varepsilon_r - 1}{\varepsilon_r} \tag{15}$$

for oxide layers as described above. Therefore the models agree well for $\omega \ll cZ_0/(b|Z_s(\omega)|)$ and differ by the factor $1/\alpha$ for $\omega \gg cZ_0/(b|Z_s(\omega)|)$. The oxide layer equations (6 - 10) hold even in the xz-case, but with $\omega_r^{(xy)} = \omega_r^{(rz)}/\sqrt{2}$. The oxide layer model for periodic protrusions works even for the xy-model with the same parameters as described before. In Fig. 8 the wakes of a surface with longitudinal periodicity are compared (solid lines). Both curves agree well for small values of s. The deviation for larger values of s reflects the difference in ω_r.

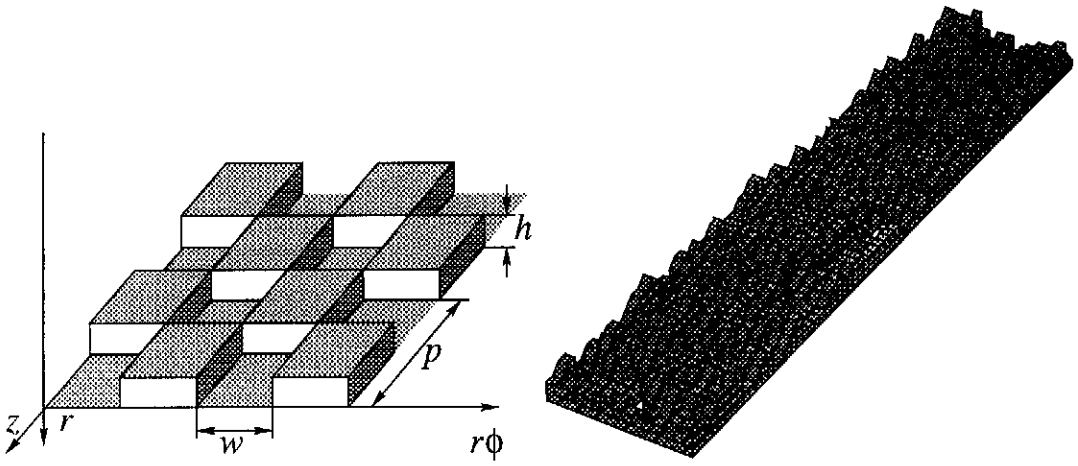

Figure 7: 3D Surface: a) periodic, b) random

3D periodic models: For a sinusoidal surface structure $x(y,z) = b + \sqrt{2}\sigma_{\text{RA}}\cos(2\pi(y\sin(\phi) + z\cos(\phi))/\lambda)$ it can be shown by perturbation theory ($\alpha < 0.1\lambda$) that the impedance at low frequencies is given by:

$$Z_{\|}(\omega) = -i\omega\frac{\mu}{b}\frac{\sigma_{\text{RA}}^2\cos^2(\phi)}{\lambda} .$$

The impedance of a structure is not only proportional to σ_{RA} but also to the ratio of RMS roughness and longitudinal wavelength $\sigma_{\text{RA}}/\lambda$. Therefore the wake of a surface as in Fig. 3 might be more then one order smaller then estimated above.

The angle ϕ takes into account the more general case of a geometric surface wave which is not parallel to the beam. If one assumes that the impedance of a random surface is the superposition of the impedances of geometric surface waves with ϕ uniformly distributed between 0 and $\pi/2$, the effective wake of a 3D surface roughness is a factor 0.5 lower than the wake of a 2D roughness. The numerical results for a periodic 3D surface structure as sketched in Fig. 7 are compared in Fig. 8. Also the principle of linearity is not valid for surface perturbations, it can be clearly seen that the magnitude of the wake depends on the 3D shape of the surface.

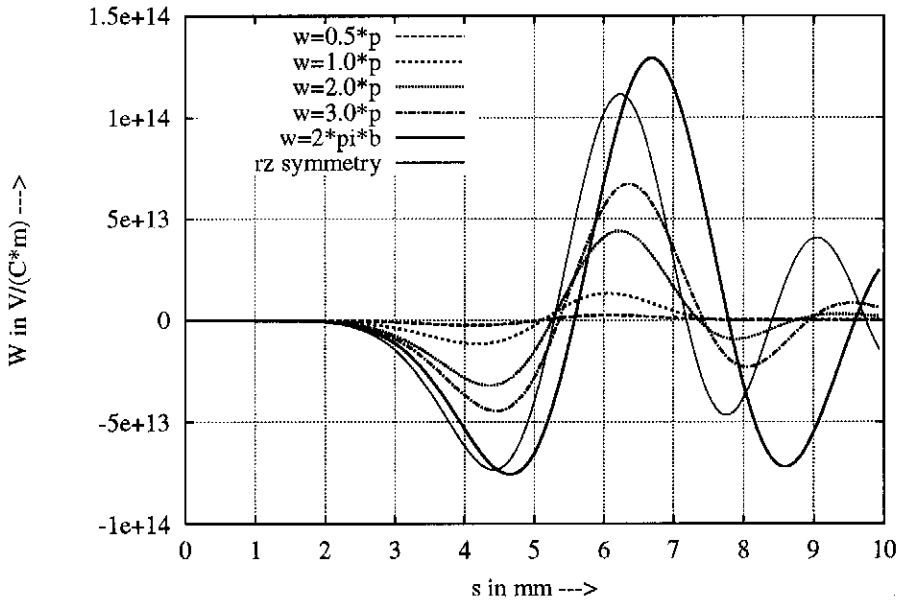

Figure 8: Wake of a periodic 3D surface (σ = 1mm, $r = 5\sigma$, $h = 0.5p = 0.13\sigma$, 1200 periods in longitudinal direction)

3D random model: The MAFIA model of a real 3D random surface is plotted in Fig. 7. This surface is characterized by the RMS magnitude $\sigma_{\mathrm{RA}} = 50\,\mu$m and the autocorrelation in both tangential directions. The autocorrelation is constant for $\sqrt{x^2+y^2} < 3\,\sigma_{\mathrm{RA}}$ and zero otherwise. To reduce the numerical effort only a piece (160 mm long, 1 mm wide) is modeled. The limited width of 1 mm corresponds to a 2 mm periodicity in azimuthal direction. In Fig. 9 the wakes of a periodic rectangular surface structure, of a 2D random surface structure and of a 3D random surface structure (all with the same σ_{RA}) are compared. The short range wakes of the 2D periodic and 2D random structure agree very well while the wake of the 3D structure is smaller by a factor of approximately 0.5 ... 0.65 as is expected from the perturbation model. For

larger values of s, the wakes of random structures do not show the oscillating behavior of periodic surfaces.

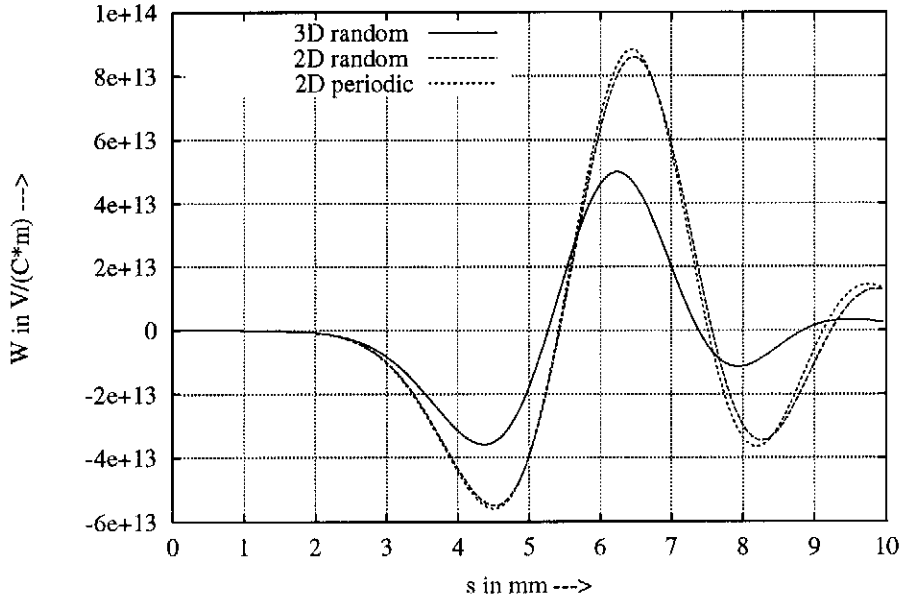

Figure 9: Wake of a rectangular xz-periodic surface, a random 2D surface and a random 3D surface

2.4.3 Summary

The 3D calculations demonstrate that the 2D dielectric layer model is essentially correct for the short range wake field. The amplitude is over-estimated by a factor of 1.5 to 2. The analysis of the 3D periodic models has shown that the amplitude of the wake potential depends not only on σ_{RA} but also on the ratio of RMS roughness and longitudinal wavelength σ_{RA}/λ. This has been not investigated in the 2D case. The amplitude of the wake potential can differ by a factor of 10 for different ratios of σ_{RA}/λ.

We consider here the worst case and calculate the peak wake for a $\sigma_z = 50$ μm long bunch according to:

$$\hat{W} = 120.7 \frac{\text{kV}}{\text{nC m}} \; 4.5 \text{ m} \; F_{3D}, \tag{16}$$

with a "3D -factor" $F_{3D} = 0.5$. The value for the 2D-case is taken from table 5.

	bunch length	
	50 μm	250 μm
one module (4.5 m)	270 kV/nC	8 kV/nC

Table 6: Approximation of peak wake potential of the contribution due to the surface roughness of 350 nm (rms) in one module.

3 Components inside each module

The block to be inserted into an undulator module which contains the beam pipe will be made of aluminum with a rectangular profile (12 mm in height). Besides the undulator pipe itself (diameter of about 10 mm) it contains the beam position monitors (BPMs) with their feed-throughs. Two different types of BPMs are under construction: Button-type and Waveguide-type monitors [13]. Their wake potential has been calculated numerically with the computer code MAFIA [4], and the results are discussed in the following sections.

3.1 Button-type Beam Position Monitors

Slightly modified commercial feed-throughs are used as electrodes ("buttons") for this monitor concept. Fig. 10 shows a cross section of the rectangular profile with the beam pipe and two electrodes of the button-type BPM [12]. The electrodes are rotated by 30 degrees with respect to the horizontal axis. Each monitor consist of four electrodes. The wake potential due to a single button-type beam

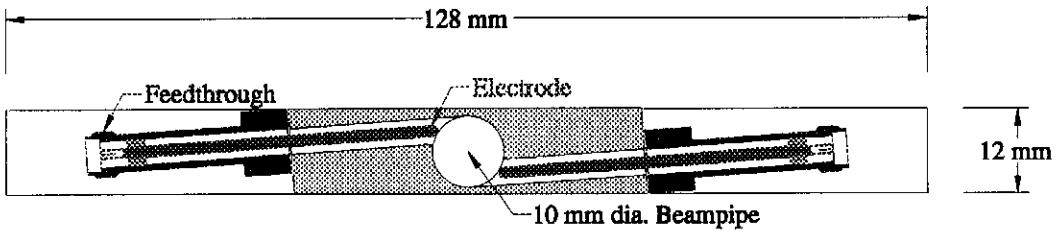

Figure 10: Button-type beam position monitor

position monitor has been calculated numerically using MAFIA [4]. One quarter of the total structure containing a single electrode (KAMAN feed-through) has been simulated. The results are summarized in table 7.

number of monitors	bunch length	
	50 μm	250 μm
single monitor, 4 electrodes	4.8 kV/nC	1.3 kV/nC
sum per module, 10 monitors	48.0 kV/nC	13.0 kV/nC

Table 7: Peak wake potential of the contribution from the button-type beam position monitors inside each undulator module

3.2 Waveguide-type Beam Position Monitors

Because of the necessarily compact size and extremely short bunches in Phase II, microwave concepts were used for the realization of a second pick-up structure [13]. In this case the magnetic field of the electron beam couples to a waveguide through a slot in the beam pipe. Four coupling slots and waveguides will be used, similar to standard electrode-type monitors. Ridged waveguides of a special shape were designed to reduce their size and to realize the coupling of about 1% at 12 GHz. At the end of each waveguide, a coaxial adapter with a vacuum feed-through is flange-mounted. The wake potetial due to a single waveguide-type

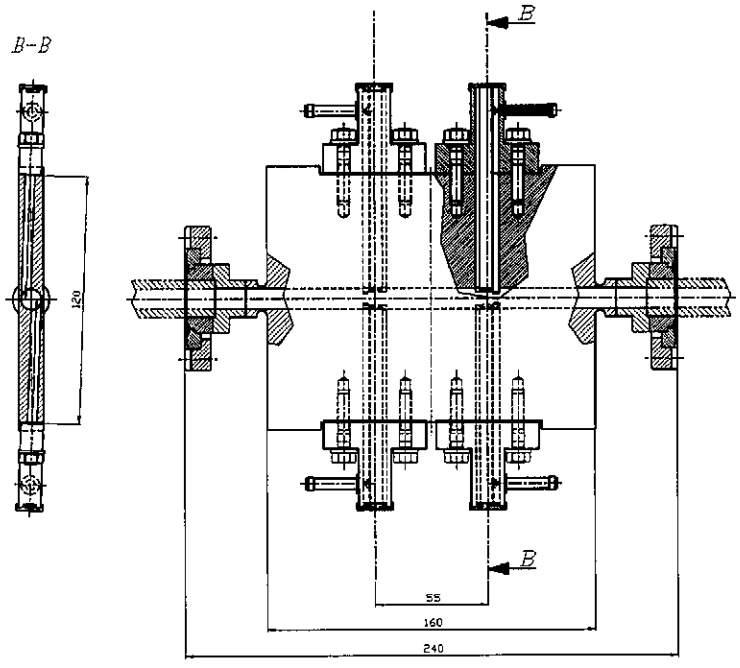

Figure 11: Waveguide-type beam position monitor

number of monitors	bunch length	
	50 μm	250 μm
single monitor, 4 waveguides	5.5 kV/nC	1.7 kV/nC
sum per module, 10 monitors	55 kV/nC	17 kV/nC

Table 8: Peak wake potential of the contribution from the waveguide-type beam position monitors inside each undulator module

BPM has been calculated numerically using the code MAFIA [4]. One quarter of the total structure containing a single waveguide with the coupling window has been simulated. The results for the prototype dimensions are summarized in table 8.

3.3 Summary

The wakepotentials of the button-type and waveguide-type monitor do not differ significantly. Both types of monitors will be used. For the impedance budget of the FEL undulator the average of both types is taken into account. The table 9 summarizes the results for one module.

	bunch length	
	50 μm	250 μm
sum per module, 10 monitors	51.5 kV/nC	15 kV/nC

Table 9: Peak wake potential of the contribution of the beam position monitors inside each undulator module (average).

4 Diagnostic Stations

A diagnostic station is located between each undulator module. Two cavity beam position monitors, two slots for wire scanners and several pumping slots contribute to the impedance of this unit. The wakefields of the cavity BPMs and the gaps for the wire scanners can be estimated from a diffraction model for a cavity gap. The wakefields due to the pumping slots are calculated numerically using the MAFIA program [4].

4.1 Cavity Gap - Diffraction model

The diffraction model gives a good description of the wakefields for short bunches. We use the results of K. Bane and M. Sands [14] to obtain the wake potential of a Gaussian bunch:

$$W_{diff}(s) = \frac{Z_0\, c}{\sqrt{2}\,\pi^2\, a}\sqrt{\frac{g}{\sigma_z}}\; F_{diff}(s/\sigma_z) \tag{17}$$

For a pipe radius of $a = 5$ mm one obtains:

$$w_a = \frac{Z_0\, c}{\sqrt{2}\,\pi^2\, a} = 1.6\ \frac{\mathrm{kV}}{\mathrm{nC}}$$

The function $F_{diff}(q)$, shown in Fig. 12, is defined as the convolution of a Gaussian bunch with the asymptotic form of the impulse wake function for small distances. It is given by:

$$F_{diff}(q) = \int_0^\infty dq'\ \frac{1}{\sqrt{2\,\pi}}\exp(-\frac{1}{2}\,(q'-q)^2)\ \ \frac{-1}{\sqrt{q'}}. \tag{18}$$

The diffraction model for a single cavity gives a $1/\sqrt{\omega}$ dependence for the broadband impedance. Only this part of the impedance is used here since the bunch length is short compared to the dimensions of the gap.

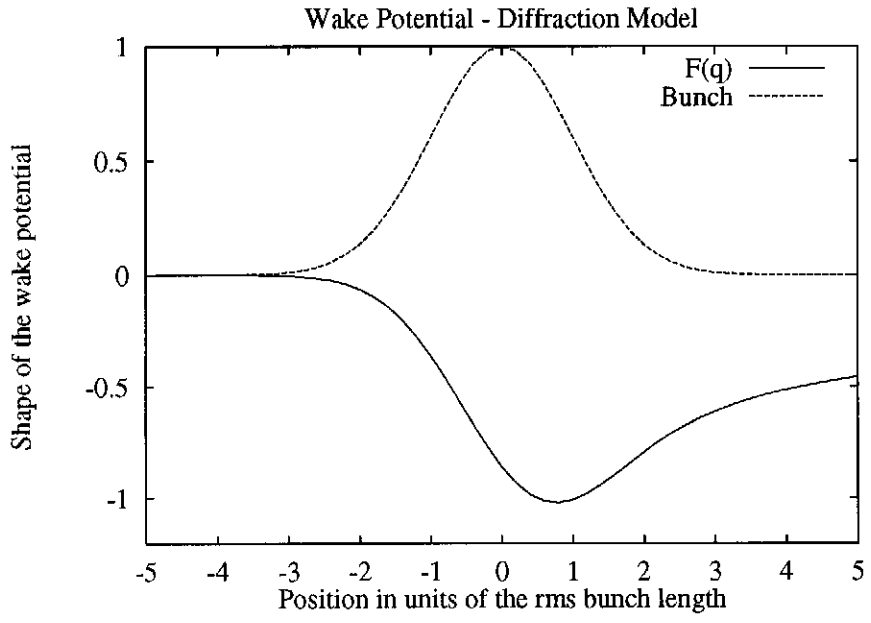

Figure 12: Wake potential - Diffraction model.

The average and the rms value of the function $F_{diff}(q)$ is approximately:

$$\begin{aligned} \langle F_{diff} \rangle &\approx -0.723 \\ \sqrt{Var(F_{diff})} &\approx 0.292 \ . \end{aligned}$$

The rms wakefield is approximately 30 % of the peak-to-peak value.

The peak wake potential $\hat{W}_{diff}$ of a cavity of length g and a Gaussian bunch with a rms length σ_z is:

$$\hat{W}_{diff} = w_a \sqrt{\frac{g}{\sigma_z}}$$

Table 10 summarizes the values of $\hat{W}_{diff}$ for the cavity monitor ($g = 9$ mm) and the gap of the wire scanner ($g = 2$ mm). The sum of the peak wake fields for one diagnostic station containing two cavities and two wire scanners is given in table 10, too.

gap length	bunch length 50 μm	250 μm
9 mm (cavity BPM)	21.5 kV/nC	9.6 kV/nC
2 mm (wire scanner)	10.1 kV/nC	4.5 kV/nC
sum per diagnostic section (two gaps of each length)		
	63.2 kV/nC	28.2 kV/nC

Table 10: Peak wake potential of the contribution from cavity and wire scanner gaps in one diagnostic section

4.2 Pumping slots

The wake potential due to pumping slots has been calculated numerically with the computer code MAFIA [4]. The grid has to be by a factor of 4 to 5 smaller than the rms bunch length to obtain numerically reliable results. An rms bunch length of 500 μm and 250 μm has been chosen for the calculations to limit the expense of computing time. The result can be scaled with the square root of the bunch length assuming the scaling law from the diffraction model for a cavity gap or by a scaling law computed from the results of the two bunch lengths. The results differ unfortunately by a factor of six.

First, the wake potential due to eight 18 mm x 2.25 mm pumping slots has been calculated. Fig. 13 shows the geometry, which has been used in the MAFIA calculation.

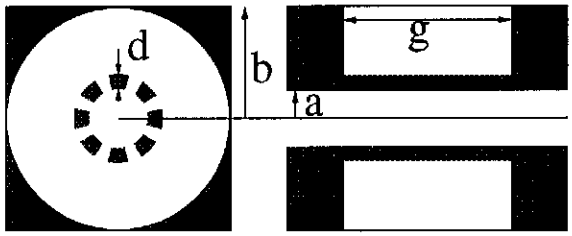

Figure 13: Pumping slots. One quarter of the geometry is calculated by MAFIA on a 86 × 86 × 281 mesh. $a = 5$ mm, $b = 17$ mm, $d = 3$ mm, $g = 18$ mm. There are eight slots with a width of $26° \cdot a = 2.26$ mm.

The wake potential for a bunch length of $500\,\mu$m is shown in Fig. 14. The peak wakefield is 0.52 kV/nC and the total loss parameter $k_{tot} = 0.26$ kV/nC. The total loss parameter is defined as $k_{tot} = \int ds W(s)\,\lambda(s)$, where $\lambda(s)$ is the line charge density of the bunch.

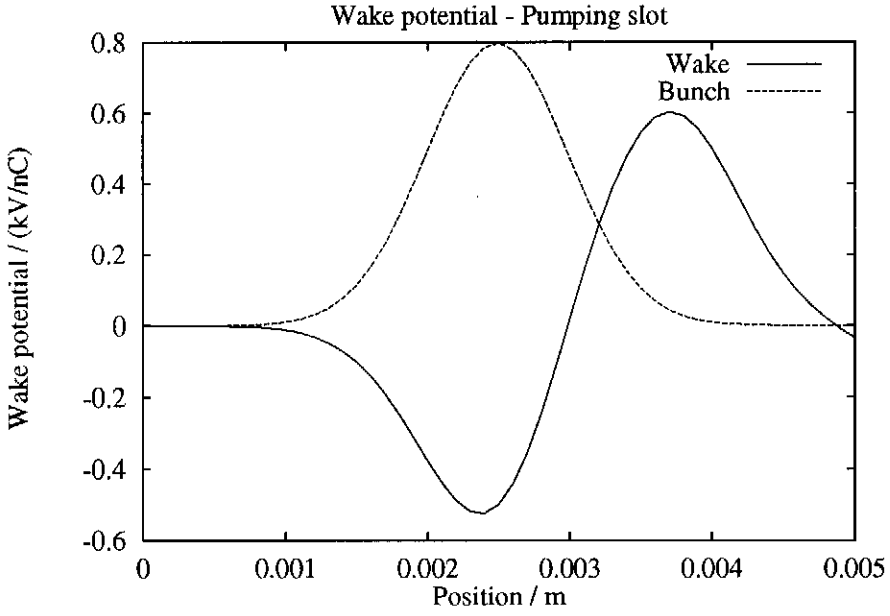

Figure 14: Wake potential, pumping slot, $\sigma = 500\,\mu$m, There are eight slots with a width of $26° \cdot a = 2.26$ mm.

The results for a bunch length of $250\,\mu$m, shown in Fig. 15, are 1.38 kV/nC for the peak wakefield and $k_{tot} = 0.85$ kV/nC. This would imply a scaling law of

$$\hat{W}_{slot} \sim {\sigma_z}^{-1.4}.$$

The expected peak value for a $50\,\mu$m long bunch is 13 kV/nC while a square root scaling would give a value of 3 kV/nC.

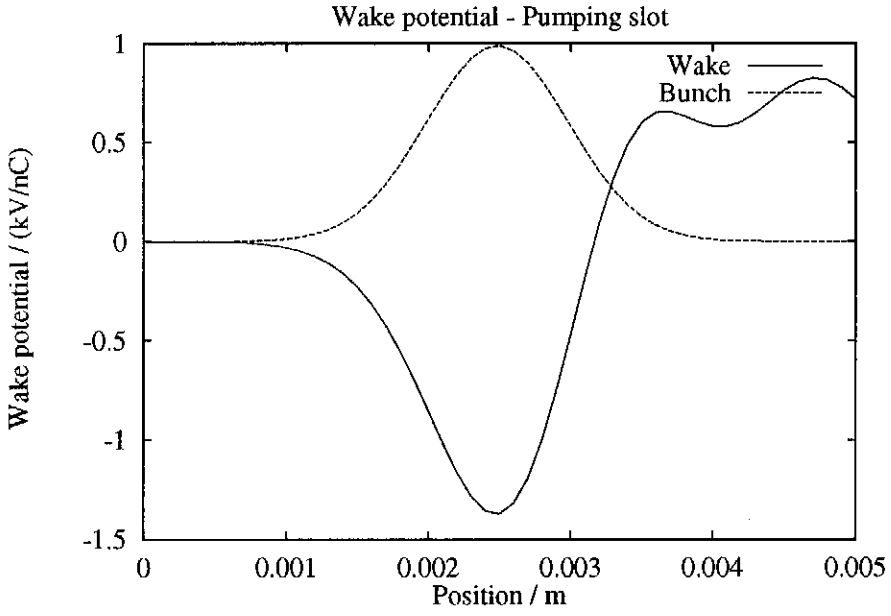

Figure 15: Wake potential, pumping slot, $\sigma = 250\,\mu$m, There are eight slots with a width of $26° \cdot a = 2.26$ mm.

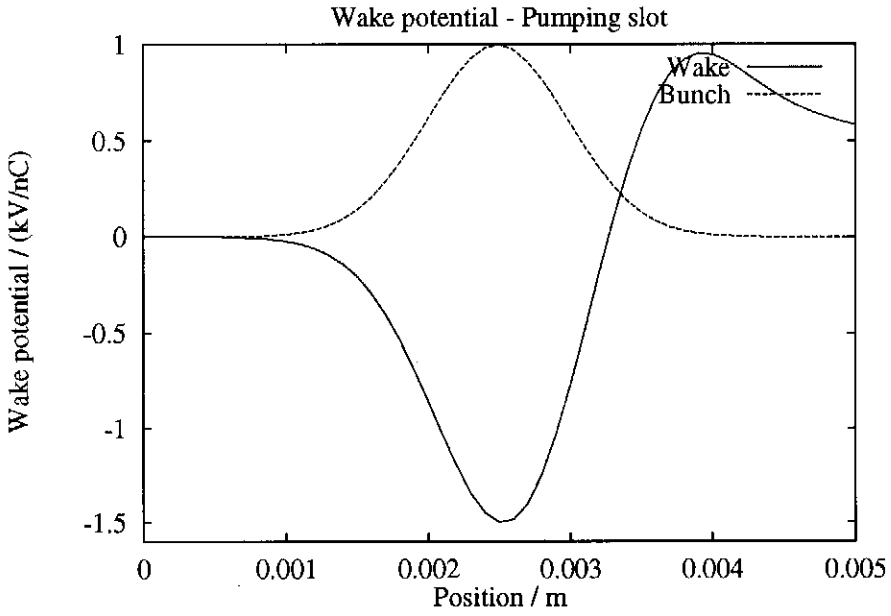

Figure 16: Wake potential, pumping slot, $\sigma = 500\,\mu$m, There are four slots with a width of $52° \cdot a = 4.53$ mm.

For a safe estimate of the wakefield effects we take the larger value. It should be mentioned that the peak wake for a cavity gap of 18 mm is 30.3 kV/nC for a bunch length of 50 μm according to the diffraction model.

Furthermore, the wake potential for four slots with double width has been calculated and the result is shown in Fig. 16. The wake is larger than for eight slots ($\sigma_z = 500\,\mu$m) by a factor of 3.

	bunch length 50 μm	250 μm
8 slots gap 18 mm	13 kV/nC (scaled)	1.38 kV/nC
per diagnostic section		
3 x	39 kV/nC	4.14 kV/nC

Table 11: Peak wake potential of the contribution from pumping slots in the diagnostic sections. The results for a bunch length of 50 μm are scaled from the calculations with a 500 μm and a 250 μm long bunch.

5 Sum of the contributions

The peak wake fields of the different objects discussed in this report are summarized in table 12. The shapes of the wake potentials differ from object to object. But the largest (negative) value of the wake potential can be found in the center of the bunch between $\pm 1.0\,\sigma_z$. The total loss parameter and the rms energy spread can be estimated from the peak wake potential $\hat{W}$ according to:

$$k_{tot} = \int ds\,\lambda(s)\; W_{\|}(s) \approx \frac{2}{3}\,\hat{W}$$

$$\sigma_E = N\,e^2 \sqrt{\int ds\,\lambda(s)\;(W_{\|}(s))^2 - k_{tot}^2} \approx \frac{1}{3}\,\hat{W}\;N\;e^2$$

Three undulator modules and three diagnostic stations are taken into account for the Phase I FEL, see Fig. 17. The wakefields in the last diagnostic section affect only the beam on its way to the beam dump.

Almost all wakefields generated in the previous section will catch up to the beam before the beam has left the last undulator section because the catch-up length L_c is short compared to the undulator length. The catch-up length L_c is

typically given by $(L_c + S)\, v_g = L_c\, c$ for a bunch of the length S. With $S = 3\sigma_z$ and the group velocity v_g for $f \simeq f_{\mathrm{RMS}}$ the catch-up length follows as:

$$L_c \simeq \frac{b^2}{\sigma_z} \ .$$

For $b = 5\,\mathrm{mm}$ and $\sigma_z = 50\,\mu\mathrm{m}$ this length is 0.5 m.

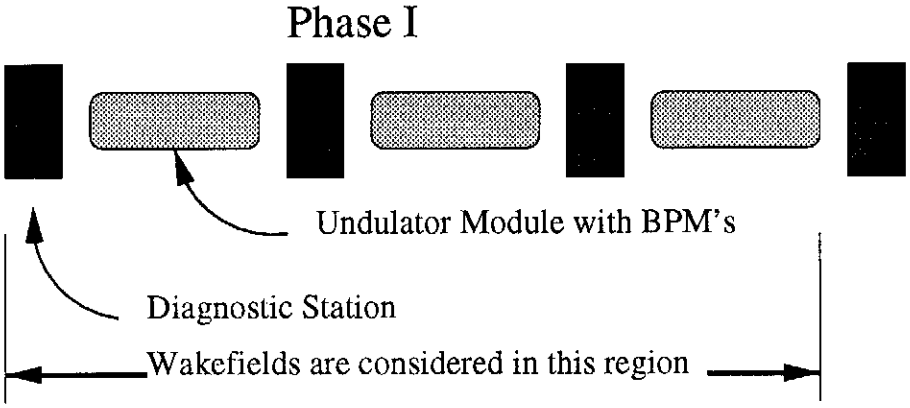

Figure 17: Schematic layout of the Phase I FEL. The last diagnostic section is not included in the estimation for the wakefield effects.

In the last line of each table the resulting energy spread at the end of the last undulator module is estimated. The peak value is given by:

$$\frac{\Delta E}{E} = \frac{\sum_i \hat{W}_i}{E},$$

with $E = 380$ MeV (Phase I) and $E = 1$ GeV (Phase II). The rms energy spread $\sigma_E/E \approx 1/3\ \Delta E/E$ is in all cases smaller than 0.1 % if the surface roughness is not taken into account, but exceeds this value in the case of a short (50 μm) bunch if the surface roughness is included in the estimate. Recent computer simulations of the SASE-FEL process [15] indicate that this does not influence the FEL gain significantly.

The impedance budget considers the main components of the FEL-undulator. Not all components are yet included. Several bellows and flanges are still missing in the budget. A planed redesign of the cavity BPM of the diagnostic stations (smaller gap), which would reduce the wakefields of that component, has also not been taken into account.

Phase I	bunch length	
3 modules, 3 diagnostic stations	50 μm	250 μm
Undulator pipe		
resistive wall	389 kV/nC	65 kV/nC
oxide layers (2 nm)	8.4 kV/nC	0.4 kV/nC
surface roughness	*$\approx$ 810 kV/nC*	*$\approx$ 24 kV/nC*
Components inside each module		
BPMs, 10 per module	155 kV/nC	45 kV/nC
Diagnostic stations		
cavities, wire scanners, 2 per station	190 kV/nC	85 kV/nC
pumping slots	117 kV/nC	12 kV/nC
Sum		
	$\approx$ 1668 kV/nC	*$\approx$ 231 kV/nC*
without surface roughness	858 kV/nC	207 kV/nC
Energy spread (peak value)		
Reference energy: 380 MeV	*$\approx$ 0.44 %*	*$\approx$ 0.06 %*
without surface roughness	0.22 %	0.054 %

Phase II	bunch length	
6 modules, 6 diagnostic stations	50 μm	250 μm
Undulator pipe		
resistive wall	778 kV/nC	130 kV/nC
oxide layers (2 nm)	16.8 kV/nC	0.8 kV/nC
surface roughness	*$\approx$ 1620 kV/nC*	*$\approx$ 48 kV/nC*
Components inside each module		
BPMs, 10 per module	309 kV/nC	90 kV/nC
Diagnostic stations		
cavities, wire scanners, 2 per station	380 kV/nC	246 kV/nC
pumping slots	234 kV/nC	24 kV/nC
Sum		
	$\approx$ 3337 kV/nC	*$\approx$ 462 kV/nC*
without surface roughness	1716 kV/nC	414 kV/nC
Energy spread (peak value)		
Reference energy: 1 GeV	*$\approx$ 0.33 %*	*$\approx$ 0.05 %*
without surface roughness	0.17 %	0.041 %

Table 12: Summary of peak wake potential of several elements in the TTF-FEL Phase I and Phase II. Additionally the peak value of the correlated energy spread is calculated for the reference energy of 380 MeV (1 GeV) for Phase I (Phase II).

Acknowledgment

We would like to thank A. Novokhatski for discussions on the dielectric layer model of the surface roughness and S.G. Wipf for carefully reading the manuscript.

References

[1] *A VUV Free Electron Laser at the TESLA Test Facility Linac - Conceptual Design Report*, DESY Hamburg, TESLA-FEL 95-03, 1995

[2] K.L.F. Bane, *The Short Range Resistive Wall Wakefields*, SLAC-AP-87, June 1991

[3] H. Schlarb, *Resistive Wall Wake Fields*, Diploma Thesis, University of Hamburg, Aug. 1997, TESLA Report 97-22

[4] T. Weiland, *On the numerical solution of Maxwell's Equations and Applications in the Field of Accelerator Physics*, Part. Acc. 15 (1984), 245-292

[5] A. Piwinski, *Longitudinal and Transverse Wake Fields in Flat Vacuum Chambers*, DESY 84-097, Oct. 1984

[6] The data for the undulator have been communicated by J. Pflüger, DESY. They are based on measurements at Argonne Nat. Lab. .

[7] D.R. Lide, H.P.R. Frederikse eds., *CRC Handbook of Chemistry and Physics*, CRC Press, Boca Raton, Ann Arbor, London, Tokyo 1994-95

[8] A. Novokhatski, and A. Mosnier, *Wakefields of Short Bunches in the Canal Covered with Thin Dielectric Layer*, to be published in the Proceedings of the PAC97, Vancouver, 1997

[9] Y.H. Chin, *Users's Guide for ABCI version 8.7: Azimuthal Beam Cavity Interaction*; CERN SL94-02 AP, 1994

[10] K. Bane, C.K. Ng, and A.W. Chao *Estimate of the Impedance Due to Wall Surface Roughness*, to be published in the Proceedings of the PAC97, Vancouver, 1997

[11] M. Dohlus, *Ein Beitrag zur numerischen Berechnung elektromagnetischer Felder im Zeitbereich*, Thesis, TU-Darmstadt 1992

[12] The button-type BPM for the undulator has been developed by M. Wendt, DESY, Hamburg

[13] R. Lorenz et.al., *Beam Position Monitors inside the FEL-Undulator at the TTF Linac*, to be published in the Proceedings of the PAC97, Vancouver, 1997

[14] K.L.F. Bane, M. Sands *Wakefields of Very Short Bunches in an Accelerating Cavity*, SLAC-PUB-4441, Nov 1987

[15] S. Reiche, private communication